Draft version May 8, 2020
Typeset using LaTeX **twocolumn** style in AASTeX63

Tidal Debris from M33: Stellar Streams of M33

José Pérez Chávez
University of Arizona

ABSTRACT

The tidal streams of M33 during and after the MW-M31 merger are investigated through a visualization pipeline that generates a multiple perspective view for the Local Group galaxy system. Tidal debris of satellite galaxies has been investigated in systems with no constraints in real data. While these papers have made conclusions that can be applied to a range of systems, these hypothesis have never been tested against a system with a non-arbitrary known state. This assessment will serve as a step forward for implementing their results to reproduce evolutionary history of any know galaxy. van der Marel et al. (2012) offers a purely deterministic Local Group kinematics evolution data set that will be used to examine the tidal interaction evolution. The visualizations proved most useful at identifying three main stages of tidal debris, and disk morphology evolution that differ in combined potential proximity, and tidal arms development. The pre-stream stage consists of impervious disk structure with little tidal interaction. The mid-stage marked the beginning of permanent disk elongations, and severe tidal tail formation, and the first stellar streams. At last the late-stage increased the amount of stellar debris that enter the potential at larger depths, and severe elongations. While the pipeline was not perfect it allowed me to estimate that at the late-stage the stellar streams approximated a depth of 32 kpc from the center of M31. These underlying evolution stages of tidal interactions, and streams prove to match works from literature, but also improves our understanding of the tidal evolution timeline in realistic system states such as the Local Group.

Keywords: galaxies: individual (M33) — galaxies: kinematics and dynamics – galaxies: stellar streams — Local Group — Jacobi Radius — Tidal Stripping/Sharing — Tidal Tails

1. INTRODUCTION

Our Milky Way (MW) galaxy is on a collision course with its neighbor, the Andromeda galaxy (M31). These two galaxies, and their respective satellite galaxies, such as M33, form our Local Group (LG). The term Local Group refers to the fact that the galaxies within our vicinity are gravitationally bound to each other (Bergh 2000). This type of system consists of bodies that do not move apart from one another as unbound galaxies do because of cosmic expansion (or the Hubble flow). The LG stellar population and kinematics can be resolved, contrary to farther galaxies, and as such is an important probe into galaxy interactions, structure, and evolution.

van der Marel et al. (2012) provided the first M31 stellar proper motion measurements, which combined with new solar motion understanding, position and velocities based on known values, concluded that the MW and M31 will merge $5.86^{+1.61}_{-0.72}$ Gyr from now. The canonical measurements served as initial conditions of their LG dynamical system simulation of particles driven purely under inter-gravitational forces, usually denoted as N-body simulations. This dataset became the first deterministic LG simulation constrained at such high degree. The collected kinematic data provides an accurate insight into the future of the MW-M31-M33 system, and becomes a realistic case study for orbital evolution, tidal, merger process, and remnant structure.

Tidal interactions between galaxies cause formation of bridge-like structures, extended spiral arms, leading or trailing tails, stellar streams (Toomre & Toomre 1972). These dynamical interactions can provide powerful constraints on a host galaxy history, their dark matter halo structure, and any progenitor satellite galaxies. Johnston & Carlberg (2016) gives an review of how stellar streams phase-space distribution constraints dark matter distribution. A great application example is our own Milky Way and the Sagittarius dwarf. The Sagittarius tidal streams have been studied and been subject to multiple attempts to constraint the overall shape of the Milky Way dark matter shape (e.g. Irwin et al. (2001); Johnston et al. (2005); Law & Majewski (2010);

Vera-Ciro & Helmi (2013)). This study also extends to the dark matter substructure such as finding subhalos (Yoon et al. 2011; Carlberg 2018). When a dark matter subhalo crosses a stellar stream, it can disrupt the stellar stream density and produce gaps, and as such constraints the subhalo relative position and potential (Johnston & Carlberg 2016). However, there is a degeneracy in the stellar stream underdensities; they can be caused by the galactic center too (Pearson 2018) [1].

The evolution of these structures can also help us better understand a galaxy's stellar distribution history, and trace the satellite galaxy progenitor. Choi et al. (2007); Amorisco (2017) implemented N-body simulations with truncated NFW spherical halo density profiles following a ΛCMD universe (Navarro et al. 1997). These simulation models were used to probe into the satellite stellar accretion, tidal tail production, and interpretation of observed streams in Milky Way-like galaxy systems. Both simulations make valid assumptions on spherical densities, and dark matter dominated systems, but they still differ in the concluded dominant forces at play, and the mass dependence scaling. Amorisco (2017) concluded that the dynamical friction erases any satellite orbital footprint in the stellar stream for satellite-to-host virial mass ratios of $\gtrapprox 1/20$. On the other hand, Choi et al. (2007) ignored any dynamical friction, and relied strongly on the torque produced by the satellite galaxy on the streams as they enter the host galaxy (Fig .1). They found that inference on the progenitor's orbit from the tidal tail is practical only for satellites for $M_s/M_h < 0.0001$. Both models agree on the fact that the most massive satellite galaxies will not serve to constraint orbital progenitor paths, and their streams will dive deeper into the host potential. Their findings on low-mass dwarf galaxies match the results of previous papers (e.g. Fujii et al. (2006)), and improve previous tidal debris tail interpretations that did not account for this mass dependency (e.g. Johnston et al. (2001)).

While Choi et al. (2007); Amorisco (2017) provide useful statistical constraints on different types of host-satellite systems, their goals were never to reproduce evolutionary history of any know galaxy. In this paper I focus on using the van der Marel et al. (2012) accurate LG phase-space data to analyze M33 stellar accretion during and after the MW-M31 merger. This realistic scenario will help us assess the discussed statistical constraints. I will investigate the stellar stream morphological evolution, as well as the correlation between the M31-M33 orbit and the stellar stream prevalence.

[1] I could not find a source for this paper, but I found a video of her presentation:https://youtu.be/HJJsIHrBBLQ

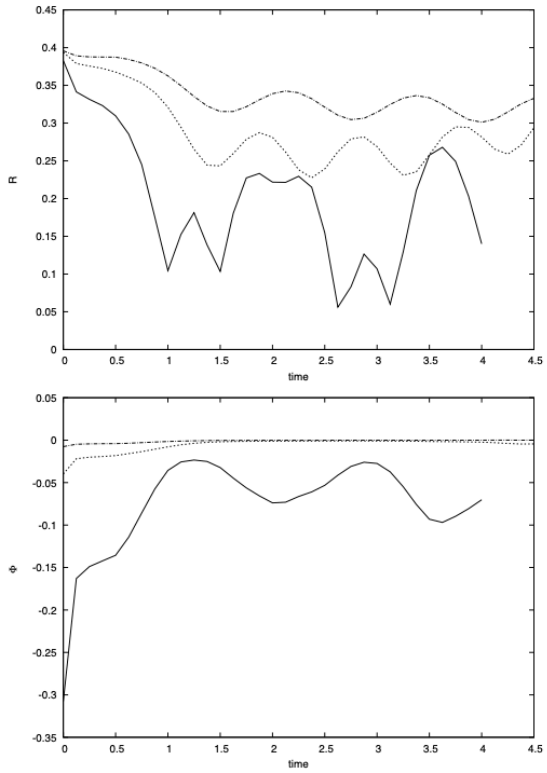

Figure 1. Choi et al. (2007) shows here the mean radius (top) and satellite potential (bottom) over time of a tail particles sample. The massive (solid line), low-mass (dotted line), and tiny- mass (dash–dotted line) satellites are plotted. Both the low-mass and tiny-mass satellite galaxy show no significant effect from the satellite's potential. On the other hand, the massive satellite generates a significant tug on the particles as its potential increases, and shows that the particles go deeper into the host potential.

2. METHODS

We are concerned in this paper with the formation, and morphology of M33 tidal streams created during, and after the the coalescence of the MW-M31 halo. We use the 802 low resolution snapshots from the van der Marel et al. (2012) dataset described in the Introduction. It provides the resolution, and particle kinematic information for the LG that we need in order to analyze the stream evolution.

2.1. *Tidal Streams*

The tidal interactions between the MW-M31 merger and M33 will generate tidal tails, and streams in all galaxies. The simulation we are working with predicts that M33 will not merge, and will remain orbiting the

MW-M31 system for the coming future. This behavior is shown in Fig. 2. During the whole process M33 will lose mass to the MW-M31 remnant, so called stellar streams. The stellar mass of M33 is lost in a tug war between the LG galaxies potentials as they get close to each other. As the smaller galaxy, M33, orbits the larger MW-M31 merger the stars in M33 feel a combined gravitational force that is changing in time. At some point in time their potentials overlap considerably, and there is an exchange of stellar mass. While this represents a complicated three body problem we can make the following assumptions, as discussed in Sparke & Gallagher (2007), to find an estimate to the distance at which M33 stars will no longer be bounded by M33:

1. The satellite follows a circular orbit,
2. The satellite potential is constant in a frame of reference rotating at constant speed,
3. The satellite's mass is much less than that of the main galaxy,
4. The main galaxy's potential can be approximated as an isothermal sphere.

Under these assumptions we can find that our system combined potential can be easily be formulated such that two of its Lagrange points become

$$r_J = \pm D \left(\frac{m}{2M\,(< D)} \right)^{1/3}, \qquad (1)$$

along the line joining the two systems. In our expression m and M are the small galaxy, and big galaxy correspondingly, and D is the distance between the two galaxies center of mass. Stars that cannot stray further from the satellite than r_J, the Jacobi radius, will remain bound to it. The Jacobi radius is sometimes referred to as the Roche limit, however it is important to point out that the Roche limit approximation is a calculation that does not take into account rotating objects (Sparke & Gallagher 2007).

While the MW-M31 and M33 system do not follow these assumptions, Eq. 1 still serves as an underestimate of M33's real Jacobi radius; the real Jacobi radius is larger due to the MW proximity. Another point to clarify is that M_{33} is not a point mass m, therefore we must determine an approximate point mass. In our work we choose $m \approx M_{33}\,(< D/2)$. We justify this estimate for long distances D with the fact that the dark matter halo is highly spherical and uniform, which indicates that M33's mass distribution approximates a point mass very well.

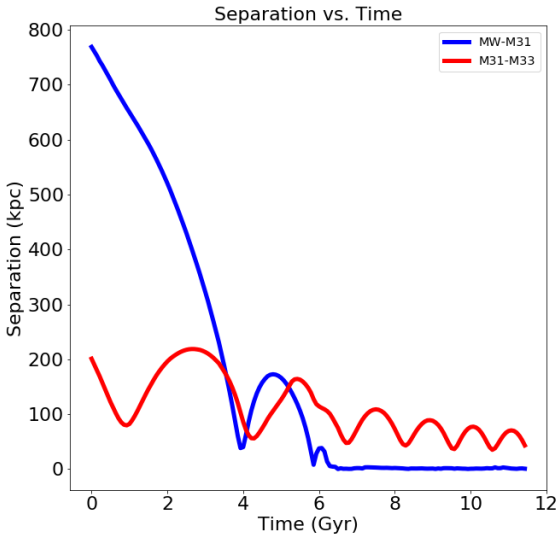

Figure 2. This plot shows the separation evolution of the MW-M31, and M31-M33 systems. While the MW-M31 system is predicted to merge approximately 6 Gyr from now, the M31-M33 system shows a slower decaying orbit. As the systems get closer, the tidal interactions increase, and considerably change M33's morphology.

We can then use this distance to keep track of all luminous particles that fall outside it. We can track all unbounded particles using Eq. 1, and keep track of any tidal streams falling into the MW-M31 remnant By measuring $r_{str} = D - r_J$ from its center of mass. We can better visualize the combined potential and its Lagrange points in Fig. 3.

In order to best qualitatively assess the changes in the disk and tail morphology over time is to visualize the data in a top Z-axis view, and cylindrical coordinates ρ and θ. In order to produce such visualization we first need to rotate the galaxies' reference frame such that the Z-axis aligns with their disk angular momentum axis, L_z. That way we can plot the top view, and use the x and y determine the ρ and θ coordinates.

We can rotate our galaxy's center of mass frame by computing its total orbital angular momentum, $\mathbf{L_{orb}} = \sum m_i \mathbf{r_i} \times \mathbf{v_i}$, mapping the normalized $\mathbf{L_{orb}}$ vector to a $\hat{\mathbf{z}}$ unit vector of the disk and setting up a rotation matrix. We can now freely use this rotation matrix to rotate each particle's position vector such that we can plot the new $\mathbf{x}'$ and $\mathbf{y}'$ vectors as a top view.

Once the we have the new reference frame oriented such that the x, y axes align with the disk we can convert to cylindrical coordinates and visualize them. We can

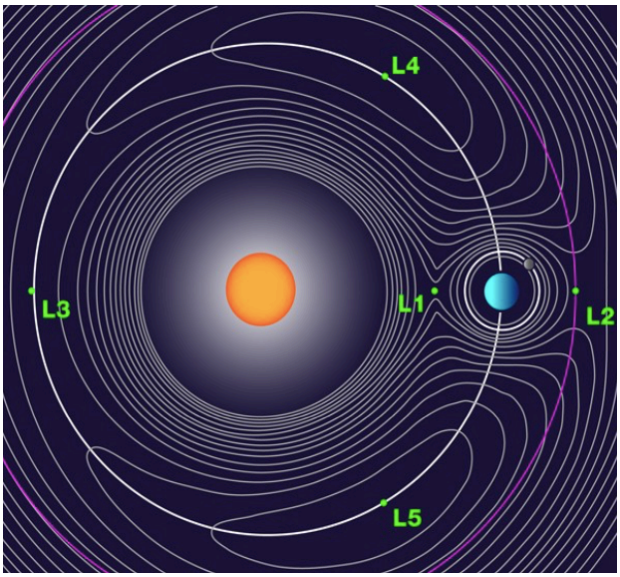

Figure 3. In this figure we can see the combined potentials of a two body system (Lectures), The Lagrange points L1-L5 are potential extrema. For close binary stars, if the outer envelope of one star expands beyond L1, its mass begins to spill over onto the other; this is the location of where our tidal streams spill into the MW-M31 remnant.

convert them using

$$r = \sqrt{x'^2 + y'^2} \qquad \text{OR} \qquad r^2 = x'^2 + y'^2, \quad (2)$$

$$\theta = \tan^{-1}\left(\frac{y'}{x'}\right). \quad (3)$$

The cylindrical view on the disk will be helpful in determining tidal tails' effective lengths and structural changes.

3. RESULTS

For preliminary results, I chose to assess the tracked stellar streams using data point visualization of the LG in different perspectives. I created a visualization pipeline in order to make preliminary conclusions on the stream morphology, such as how much the streams delve into the potential, and their orbit type around the merger remnant. In order to achieve this my visualization pipeline offers four different dynamic visualization perspectives:

1. A scatter density map from positive Z-axis view of each isolated galaxy,
2. A scatter plot of unfolded ρ and θ cylindrical coords of each galaxy,
3. Scatter density maps of each galaxy centered in M33's center of mass,
4. A scatter density map of the M31-centered tidal streams within $r = D - r_J$.

Each visualization technique give us different insights into the evolution of the MW-M31 and M33 system, and the tidal streams. The top Z-axis views demonstrate the deformations on the disk-like structures of each galaxy, and the tidal tail formation of all galaxies over the span of 10 Gyr. The cylindrical views give a better sense of scale for the formation of tails, and how far they extend in the $\hat{\rho}$ direction. The density maps together in one plot are good for exploring the correlation between the interactions timeline, and the other plots features. The last density map showcases the M33 tidal streams which helps us infer on their morphology, and orbits, with addition to the M31 as a background to give a sense of scale. The presented outputs of the visualization pipeline are included in the Appendix.

Here we present three main stages of the tidal stream evolution. In the pre-streams stage we observe tidal interaction between all galaxies that do not produce permanent tidal tails. The first presence of tidal pulls on M31 and M33 happen shortly after their first pericenter, at approximately $t - 1428$ Myr. We can easily observe the tidal features in the cylindrical view, two main overdensities peaking towards $12\hat{\rho}$ kpc. We can also observe two bump-like features on M31 peaking at approximately $42\hat{\rho}$ kpc. At this age, MW is still at least at a distance of $\approx$ 500kpc from M31 and M33. Three Gyr after, shortly after the MW–M31 first-pericenter time, I observed the first unbounded M31 stars within a distance of 50 kpc from M31. Due to the high proximity of all galaxies, we can observe high tidal interactions on all galaxies; MW shows two main $45\hat{\rho}$kpc tidal tails, and both M33 and M31 display high ellipticity. This stage lasts a few Gyr until the first pericenter of the MW-M31 orbit, and is displayed in Fig. 4.

Once the MW-M31 orbit has completed their first pericenter the galaxies' tidal interactions start producing a permanent elongation on M33's disk, as well as more pronounced tidal tails. A major tidal stream is observed beginning to orbit M31 at $t = 5400$ Myr with a stepp entrance on the bottom right plot in Fig. 5. By the time MW-M31 merge, at $t = 5.86^{+1.61}_{-0.72}$, the galaxies have already suffered great deformation including M33's tidal arms, observed in both plots in Fig. 5, referred to as the mid-stage. Also, we can observe a greater amount of stream stars within 50 kpc from M31.

For the next Gyr all galaxies' disks spread outward as the exchanges of tidal streams, and deformations settle onto the disk angular momentum axis. By the time $t = 8470$ Myr M33 tidal arms have extended up to 280

kpc. The top Triangulum top view in Fig. 6 shows the large tidal tail going inwards, and curving around M31, better observed on the bottom right plot. This tidal arm arches and produces a large stellar stream across MW-M31 remnant combined halo. We can also observed extended disks for the MW-M31 remnant. This last stage is showcased in Fig. 6.

4. DISCUSSION AND CONCLUSION

My visualization pipeline proved useful at qualitatively analyzing the van der Marel et al. (2012) LG low resolution phase-space data to explore the accurate evolutionary path of our LG galaxies' morphology changes, and stellar accretion during and after the MW-M31 merger.

The stellar stream morphology evolution was discussed in great detail in Sec. 3. We discussed the three main stages, and their key differences. That way recreating a three-stage timeline of the stellar stream creation. We also discussed the effect of the proximity of each galaxy, and their impact in the tidal tail evolution during the merger. The decaying orbit of M31 drove most of the tidal interactions of the system, and the removal of stellar mass from M33. However, the stellar streams density map did not do a good job at allowing us to infer the depth at which this stellar mass entered the MW-M31 remnant. The static reference frame really only shows one view with no sense of depth (third axis), so it is hard to convey distance correctly. However, we can further analyze both the top and cylindrical views on M33. The top view displays a tidal arm curving at almost a constant ρ value in the last stage of the system. The cylindrical view also shows a horizontal bridge which matches the curved arm feature. This horizontal bridge is at $\rho \approx 32$kpc, less than the pre-streams disk extents, and an even smaller fraction of the late-stage MW and M31 tidal arm lengths. This length certainly shows that the tidal arm is at least one-third into the remnant potential. While my visualization pipeline does not allow me to investigate the efficiency of M33 orbital path inferring based on the streams, it very well proved that, M33 (a massive satellite) spilled stellar debris that fell deep into the potential, as expected from Amorisco (2017); Choi et al. (2007).

The r_J estimate proved to produce variable results as the number of particles within the Jacobi radius increased and decreased at different t times throughout the simulation. Using the stream tracking technique discussed in Sect. 2.1 did not produce a consistent radius at which stars that spilled out would not return; inconsistent number of unbounded particles. In order to increase the accuracy of my Jacobi radius, and therefore a consistent trend of unbounded particles, I need to use the higher resolution dataset as it will give me a better measurement of the Jacobi radius. Also, Eq. 1 assumptions are only good approximations at large D as discussed in Sec.2. Therefore, I should use a more general approach at runtime in order to accurately calculate the Jacobi radius.

5. ACKNOWLEDGMENTS

Thanks to Gurtina Besla for her mentorship, and guidance throughout the project, as well as Rixin Li for his suggestions and supervision in code check ins. This research made use of Astropy, [2] a community-developed core Python package for Astronomy (Astropy Collaboration et al. 2013; Price-Whelan et al. 2018). The project made use of the JupyterLab environment [3] to prototype and perform all tasks (Kluyver et al. 2016). We made use of several other packages such as Scipy, Numpy and Matplotlib (Oliphant 2007; Hunter 2007; van der Walt et al. 2011; Virtanen et al. 2020). Lastly, we made great use of an indepedent extension of Matplotlib to create scatter density maps[4].

APPENDIX

This appendix's sole purpose is to showcase our visualization pipeline outputs. The visualization pipeline's main purpose is to animate the evolution of the LG, but we manage to extract frames to present on this static format. The visualization pipeline was designed using the methodology described in Sect. 3 and implemented using Python, matplotlib as the main plotting package and the mpl-scatter-density extension package. The design of the canvas is customized at the initialization of the visualization pipeline with the dimensions chosen through experimental space optimization. All scatter density data was plotted using custom colormaps that enabled more than one galaxy to be plotted at the time in a single Axes. The pipeline makes consistent use of a purple-yellow colormap for MW, a

[2] http://www.astropy.org

[3] https://github.com/jupyterlab/jupyterlab

[4] https://github.com/astrofrog/mpl-scatter-density

green-violet colormap for M33 and a red-yellow colormap for M33. The first few Gyr of the system show low resolution density maps on the lower left plot due to the fact the animation's the dynamic axes start at long ranges, and are reduced as time goes on. These minimalist plots display at most two tick labels per axis in units of kpc. The unfolded cylindrical plots are shown with the Y-axis to be the inverted ρ coordinate, and the X-axis the θ coordinate.

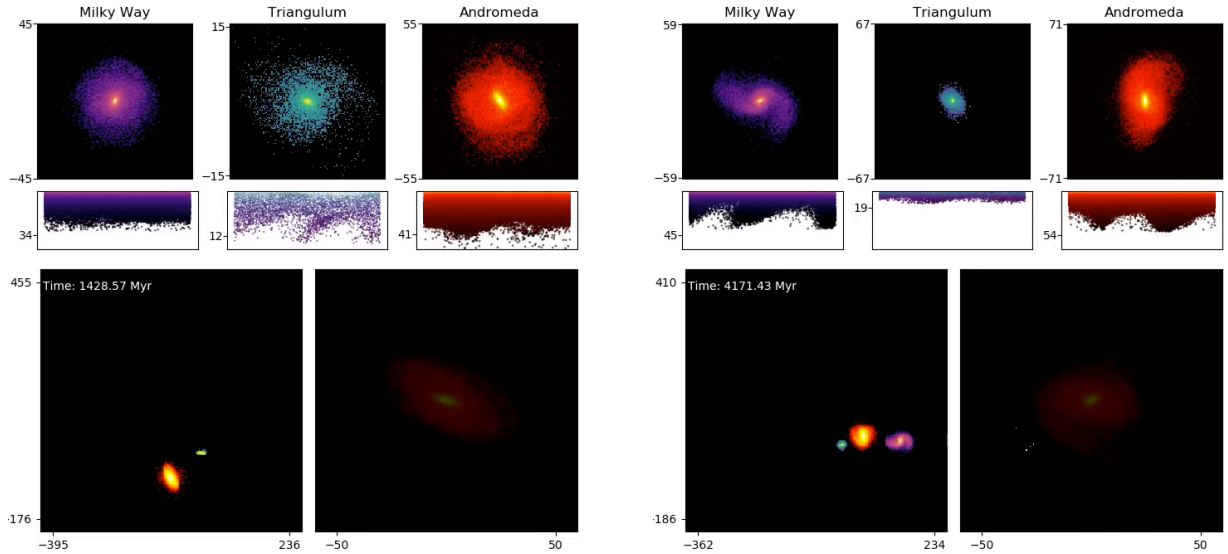

Figure 4. In this figure we see output of the visualization pipeline for $t - 1428$ and $t = 4171$ Myr. On the left side we see the effect of the first M31-M33 orbit pericenter, which happens on $t = 0.85^{+0.18}_{-0.13}$ Gyr (van der Marel et al. 2012). After 500 Myr the potential interactions produce small tidal tails on M33, and disk-bumps on M31. On the right side we see the first stellar spill towards M31 produced shortly after the MW–M31 first-pericenter time, $t = 3.87^{+0.42}_{-0.32}$, on the bottom right subplot.

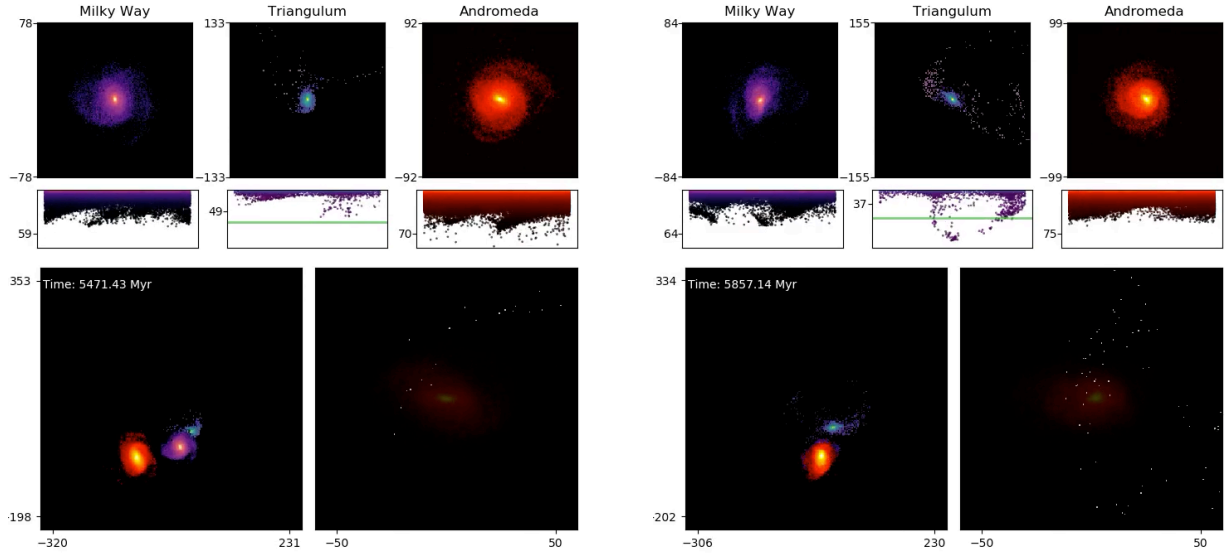

Figure 5. On the left side we observe the first complete tidal stream arching and traveling towards the M31 potential. We can also observe growing tails on MW and M31. Shortly after, as MW and M31 begin the merging process around $t = 5857$ Myr (van der Marel et al. 2012), the M33 tidal tails become more prominent.

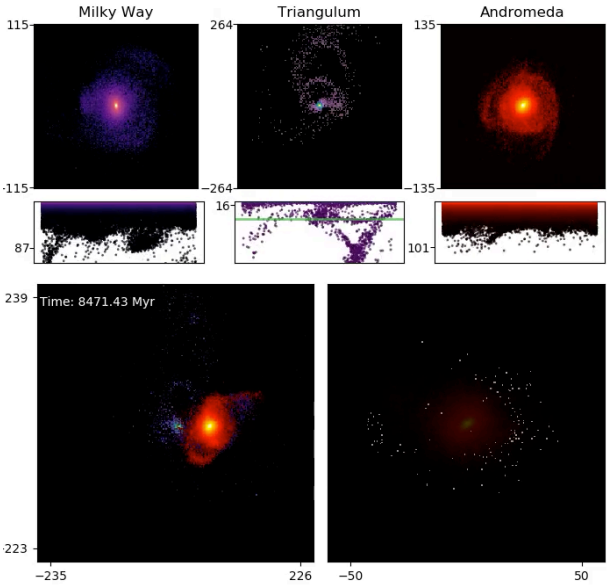

Figure 6. In this figure we can see the visualization pipeline output at $t = 8471$ Myr, 2.6 Gyr after the MW-M31 merging process begun. We observe drastic changes in M33 disk morphology. The disk now has two long tidal tails, and one arches inwards into M31. On the bottom right plot we can see there is a more clear stream orbiting across the MW-M31 remnant.

REFERENCES

Amorisco, N. C. 2017, MNRAS, 464, 2882, doi: 10.1093/mnras/stw2229

Astropy Collaboration, Robitaille, T. P., Tollerud, E. J., et al. 2013, A&A, 558, A33, doi: 10.1051/0004-6361/201322068

Bergh, S. 2000, The Galaxies of the Local Group

Carlberg, R. G. 2018, arXiv e-prints, arXiv:1811.10084. https://arxiv.org/abs/1811.10084

Choi, J.-H., Weinberg, M. D., & Katz, N. 2007, MNRAS, 381, 987, doi: 10.1111/j.1365-2966.2007.12313.x

Fujii, M., Funato, Y., & Makino, J. 2006, PASJ, 58, 743, doi: 10.1093/pasj/58.4.743

Hunter, J. D. 2007, Computing in Science Engineering, 9, 90

Irwin, M. J., Ferguson, A., Tanvir, N., Ibata, R., & Lewis, G. 2001, The Newsletter of the Isaac Newton Group of Telescopes, 5, 3

Johnston, K. V., & Carlberg, R. G. 2016, Astrophysics and Space Science Library, Vol. 420, Tidal Debris as a Dark Matter Probe, ed. H. J. Newberg & J. L. Carlin, 169, doi: 10.1007/978-3-319-19336-6_7

Johnston, K. V., Law, D. R., & Majewski, S. R. 2005, ApJ, 619, 800, doi: 10.1086/426777

Johnston, K. V., Sackett, P. D., & Bullock, J. S. 2001, ApJ, 557, 137, doi: 10.1086/321644

Kluyver, T., Ragan-Kelley, B., Pérez, F., et al. 2016, Jupyter Notebooks – a publishing format for reproducible computational workflows, 87–90, doi: 10.3233/978-1-61499-649-1-87

Law, D. R., & Majewski, S. R. 2010, ApJ, 714, 229, doi: 10.1088/0004-637X/714/1/229

Navarro, J. F., Frenk, C. S., & White, S. D. M. 1997, ApJ, 490, 493, doi: 10.1086/304888

Oliphant, T. E. 2007, Computing in Science Engineering, 9, 10

Pearson, S. 2018, in American Astronomical Society Meeting Abstracts, Vol. 231, American Astronomical Society Meeting Abstracts #231, 212.03

Price-Whelan, A. M., Sipőcz, B. M., Günther, H. M., et al. 2018, AJ, 156, 123, doi: 10.3847/1538-3881/aabc4f

Sparke, L. S., & Gallagher, III, J. S. 2007, Galaxies in the Universe: An Introduction, 2nd edn. (Cambridge University Press), doi: 10.1017/CBO9780511807237

Toomre, A., & Toomre, J. 1972, ApJ, 178, 623, doi: 10.1086/151823

van der Marel, R. P., Besla, G., Cox, T. J., Sohn, S. T., & Anderson, J. 2012, ApJ, 753, 9, doi: 10.1088/0004-637X/753/1/9

van der Walt, S., Colbert, S. C., & Varoquaux, G. 2011, Computing in Science Engineering, 13, 22

Vera-Ciro, C., & Helmi, A. 2013, ApJL, 773, L4, doi: 10.1088/2041-8205/773/1/L4

Virtanen, P., Gommers, R., Oliphant, T. E., et al. 2020, Nature Methods, 17, 261, doi: https://doi.org/10.1038/s41592-019-0686-2

Yoon, J. H., Johnston, K. V., & Hogg, D. W. 2011, ApJ, 731, 58, doi: 10.1088/0004-637X/731/1/58